

INSTABILITY OF AN INTERFACE BETWEEN STEEL LAYERS ACTED UPON BY AN OBLIQUE SHOCK WAVE

O. B. Drennov, A. L. Mikhailov,

UDC 534.222.2

P. N. Nizovtsev, and V. A. Raevskii

This paper reports results of experiments in which development of instability was observed on the interface between two identical metals in tight contact with passage of an oblique shock wave through it. Numerical modeling of experimental results was performed by a two-dimensional Lagrangian procedure using an elastoplastic model with a functional dependence of the dynamic yield point on the state variables of the material. The calculations showed that perturbations develop only in the presence of a technological microgap of several tens of micrometers between the metal layers. Unloading of the material behind the oblique shock front into the gap gives rise to a considerable short-term velocity gradient. Simultaneously, near the interface behind the wave front there is a short-term loss of strength of the material due to thermal softening and the heterogeneous nature of the deformation.

Key words: *instability, interface, oblique shock wave, strength.*

Introduction. Hydrodynamic instabilities on interfaces between materials are of great theoretical and practical interest. The instabilities of interfaces between dissimilar materials under high-velocity flow conditions have long been known and have been studied on the bases of classical continuum mechanics. These studies are of interest for various modern engineering applications, for example, for the solution of the problem of inertial thermonuclear fusion. In particular, Kelvin–Helmholtz instability (shear instability) arises when the tangential velocity-field component undergoes a discontinuity in a continuous medium, resulting in an exponential growth of perturbations on the velocity-discontinuity surface [1].

Hydrodynamic instabilities have been adequately studied for liquids and gases. However, no adequate models have been developed to describe the development of instability in media possessing strength, compressibility, and viscosity, in particular, in metals.

Numerical modeling of instability development at an interface between metals under high-velocity oblique collision was attempted in [2]–[4]; hypersonic conditions with oblique shock waves attached to the collision point were studied in [5].

Development of perturbations at an interface between two metal specimens upon passage of a shock wave with the front propagating at an angle to the interface (oblique shock wave) is most interesting in the case of identical materials. In the case of dissimilar materials, the conditions of Richtmyer–Meshkov and Kelvin–Helmholtz instabilities and, at an appropriate density ratio, Rayleigh–Taylor instability are satisfied. If two layers of the same metal are in tight contact (lack of a gap), the interface should be stable. Indeed, if shear strength is ignored, such an interface is fictitious, and flow singularities should not arise after shock-wave passage. If shear strength cannot be ignored, slippage of one layer relative to the other along the interface is possible.

A special case of instability development is the experimentally observed development of periodic perturbations on an interface between specimens of the same metal with passage of an oblique shock wave through it [6, 7].

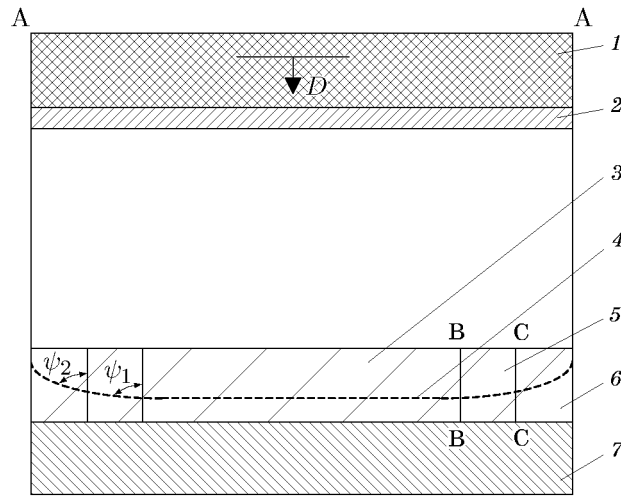


Fig. 1. Loading diagram: 1) explosive charge; 2) impactor; 3) disk; 4) shock-wave profile in the specimens; 5) ring; 6) holder; 7) bottom plate.

Analytical investigation of the process shows that if the metal layers are in tight contact, a velocity gradient on the boundary is absent and perturbation propagation does not occur. Nevertheless, experiments revealed growth of perturbations on the boundary between the metals, probably because of the presence of a microgap between the real surfaces.

The present paper reports results of experiments in which perturbations developed on an interface between specimens tightly pressed together and loaded by an oblique shock. In addition, the paper gives results of numerical simulation of the indicated process that describe instability of the interface.

Experimental Setup. Experimental Results. A loading diagram is given in Fig. 1. A disk from St. 3 steel (diameter 64 mm and thickness 14 mm) was enclosed in a ring (inner diameter 64 mm, outer diameter 90 mm, thickness 14 mm), which, in turn, was placed in a holder (inner diameter 90 mm, outer diameter 120 mm, and thickness 14 mm). The disk, ring, and holder were mounted on a bottom plate (diameter 120 mm and thickness 20 mm). The holder and bottom plate were intended to protect the disk and the ring from the destructive action of the lateral and rear rarefaction waves. All the above-mentioned parts of the experimental setup are made of St. 3 steel.

The specimens were loaded by a brass impactor 2–3 mm thick and 120 mm in diameter (impactors of different thickness were used in different experiments), which was accelerated by explosion products from detonation of a 50/50 TNT/RDX explosive charge 20–40 mm thick and 120 mm in diameter (charges of different thickness were used in different experiments). A plane detonation wave was generated simultaneously over the entire outer surface of the explosive charge (section A–A in Fig. 1). According to estimates obtained using P – u diagrams and one-dimensional gas-dynamic calculations, the shock pulse pressure at the entrance to the specimens was $P = 40$ – 55 GPa. Considering the pulse decay, the pressure at the exit from the specimens was $P = 36$ – 49 GPa.

For a loading pressure $P \approx 13$ GPa for St. 3 steel, account should be taken of the effect of a phase transition and the presence of an “impact” rarefaction wave. The chosen pressure range of shock-wave loading allows experiments to be performed with the material in a stable state. The process of perturbation development is short-term (a few microseconds) and is completed before the beginning of the reverse phase transition. Therefore, the abnormal behavior of St. 3 steel exhibited at $P \approx 13$ GPa can be ignored.

Under the action of a lateral rarefaction wave, the impactor in flight takes a curved shape (the edges lag behind the central zone). The shock-wave front is shown by a dashed curve in Fig. 1. Thus, the contact boundaries of the examined specimens (sections B–B and C–C) are loaded by an oblique shock wave.

In all experiments, the development of perturbations was observed on the disk–ring interface (section B–B) and the ring–holder interface (section C–C). Figure 2 gives photographs of microsections of the ring–holder interface (D_s is the velocity of the shock-wave front in the metal and ψ_2 is the slope of the front to the ring–holder interface).

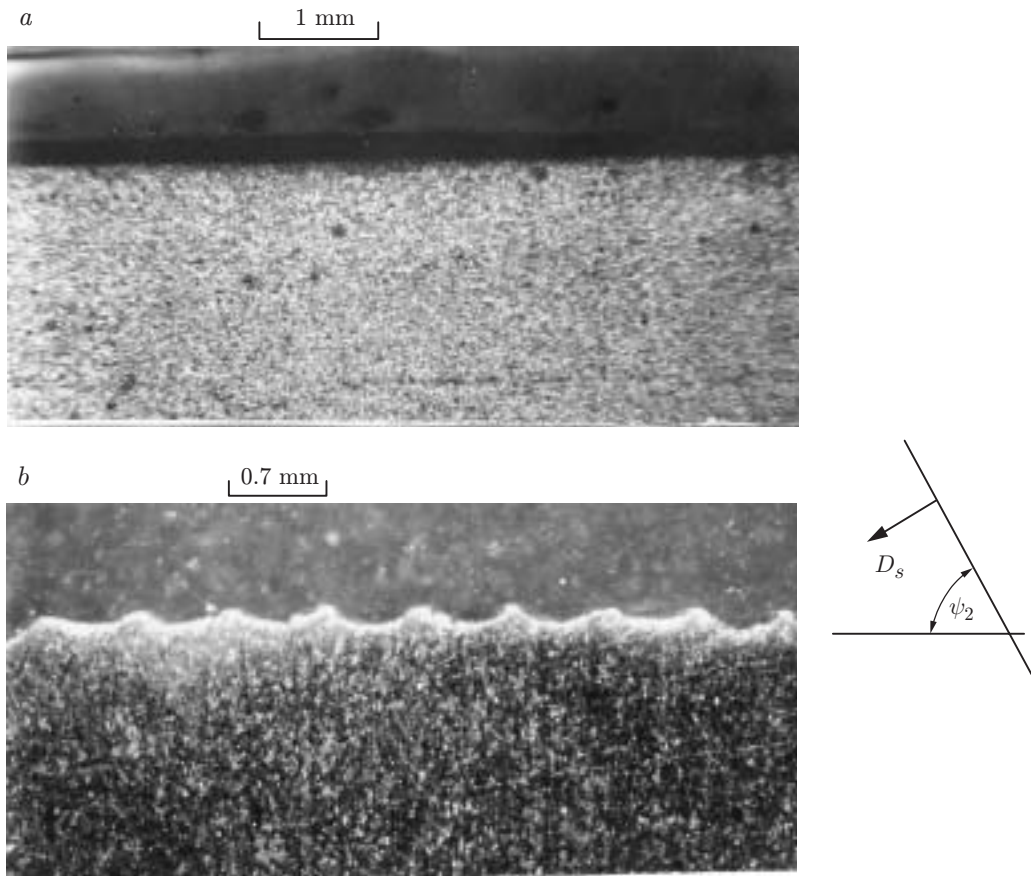


Fig. 2. Photographs of microsections of the ring-holder interface ($\times 20$): (a) the starting contact boundary of the ring (even surface); (b) contact boundary of the ring after shock-wave loading.

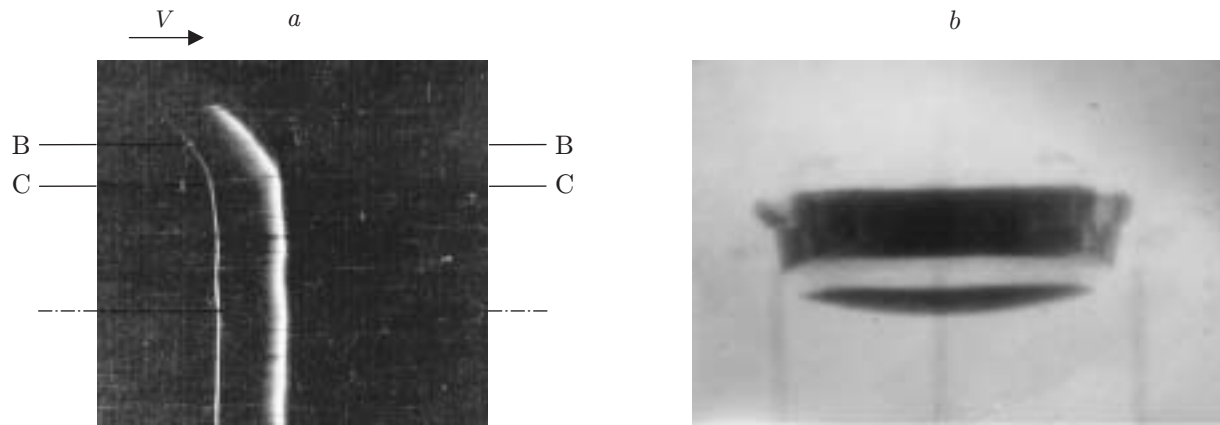


Fig. 3. Streak records(a) and an x-ray photograph (b) of the loading process by the diagram presented in Fig. 1.

The nearly sinusoidal perturbations have an amplitude $a \approx 0.06$ mm and a wave length $\lambda \approx 0.7$ mm. An drastic change of the starting structure of the steel is observed in the near-interface zone with a width $\Delta \approx 0.02$ mm.

The shape of the shock-wave pulse entering the specimens was studied in a separate series of experiments. The free-surface profile of the flying impactor was recorded at the moment of impact on the disk-ring-holder system using a high-speed SFR-2M photorecorder operating in a streak mode (so-called flash-gap method [8]). A typical shock-wave front shape at $P \approx 45$ GPa is presented in Fig. 3a.

From results of processing typical streak records it follows that the shock wave enters the disk–ring interface at an angle $\psi_1 \approx 80^\circ$ and the ring–holder interface at an angle of $\psi_2 \approx 70^\circ$ (see Fig. 1). Therefore, the interface is loaded by an oblique shock wave.

For a more detailed examination of the mechanism of relative displacement of the metal layers, the dynamic loading of the system and its subsequent motion were recorded on x-ray photographs at various times. Separate phases of motion of the elements of the system can be determined after arrival of the shock wave at the rear surface of the bottom plate. The mean velocity of motion of the ring relative to the holder is $\Delta U \approx 0.1 \text{ mm}/\mu\text{sec}$. After the ring is detached from the holder under the action of a lateral rarefaction wave, they fly by inertia at a mean velocity $\Delta U \approx 0.04 \text{ mm}/\mu\text{sec}$. A decrease in the velocity ΔU is due to the spall fracture of the bottom plate. The spalled fragment takes most of the kinetic energy of the system. Figure 3b shows an x-ray photograph of the system at the stage of inertial flight.

Numerical Simulation of the Loading Process. The passage of an oblique shock wave through an interface between two identical metal specimens was studied by numerical calculations using a two-dimensional Lagrangian procedure [9]. The shock-wave parameters and the orientation of the front relative to the interface correspond to the data of the experiment in which perturbation growth was observed. The shock front pressure is $P = 45 \text{ GPa}$. The shock wave entered the interface an angle $\psi = 70^\circ$.

The numerical simulation was performed using an elastoplastic model with a functional dependence of the dynamic yield point on the state variables of the material (plastic strain rate, pressure, temperature). The relationship between the spherical components of the strain and stress tensors was derived using the Mie–Grüneisen equation of state:

$$P = P_c + P_{\text{th}} = (\rho_0 c_0^2 / n)(\eta^n - 1) + \Gamma \rho E_{\text{th}}, \quad \eta = \rho / \rho_0, \quad \Gamma = \Gamma_\infty + (\Gamma_0 - \Gamma_\infty) / \eta^m.$$

Here ρ_0 is the density at $T = 0$, c_0 is the volume velocity of sound at $T = 0$, Γ is the Grüneisen coefficient dependent on density, $E_{\text{th}} = c_V T$ is the thermal energy, where $T > T_D$ (T_D is the Debye temperature). The elastic component of the internal energy is expressed as

$$E_c = \int P_c \frac{d\eta}{\eta^2}.$$

The relationship between the stress-deviator components σ'_{ij} and the elastic-strain deviator components ε'_{ij} is given by the relations

$$\sigma'_{ij} = 2G\varepsilon'_{ij}.$$

The shear modulus G is calculated from the formula

$$G = \frac{3(1 - 2\nu)}{2(1 + \nu)} \rho c_V^2,$$

where $c_V^2 = (\partial P / \partial \rho)_S$ is the volume velocity of sound in the compresses state and ν is Poisson's constant. The dependence of ν on the state variables is determined by analysis of experimental data on the relation between the longitudinal c_L and volume c_V velocities of sound in the shock-compressed state:

$$\nu = (3 - (c_L / c_V)^2) / (3 + (c_L / c_V)^2).$$

The melting point is determined from the Lindemann law at constant heat capacity

$$\frac{d(\ln T_m)}{d(\ln \rho)} = 2(\Gamma - 1/3).$$

The dependence of the dynamic yield point Y_d on the pressure P , plastic-strain rate ε_i^p , and temperature T is given by

$$Y_d = (Y_0 + \alpha P)(1 - E_{\text{th}} / E_m).$$

where $Y_0 = 0.45 \text{ GPa}$, $\alpha = 0.05$ are constant values, and E_m is the energy of melting of the material.

The geometry of the computational domain (Fig. 4) was close to the geometry of the experimental assembly. On the boundaries $y = 0$ and $y = L_2$, we imposed the rigid-wall condition. In the zone of interfaces, the characteristic size of the computational mesh is $5 \mu\text{m}$. An oblique shock wave was simulated by constant pressure on the left boundary of the computational domain $P = 45 \text{ GPa}$; i.e., in the computational scheme, a shock wave with a constant pressure P at the front was formed at the time $t > 0$. The calculations were performed for various

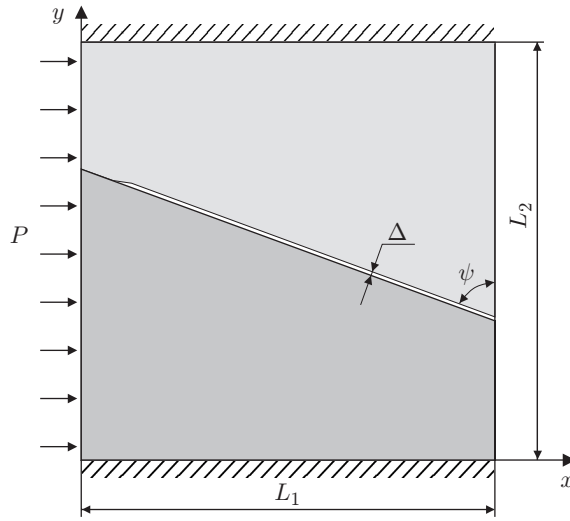


Fig. 4. Computational domain ($P = 45$ GPa, $L_1 = L_2 = 5$ mm, and $\psi = 70^\circ$).

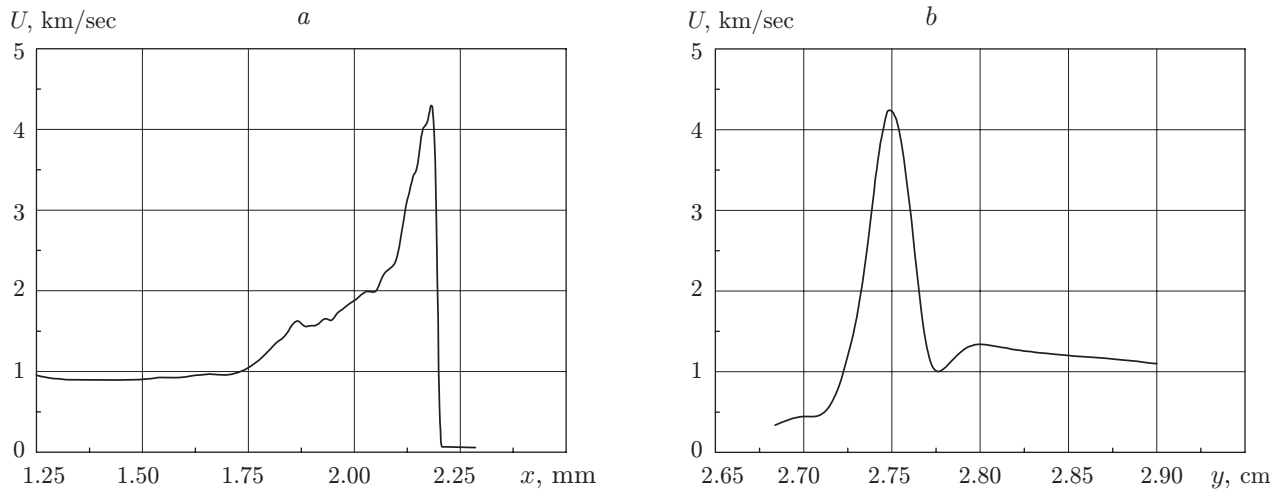


Fig. 5. Relative velocity of the material along the interface ($\Delta = 40 \mu\text{m}$): (a) projection onto the x axis; (b) projection onto the y axis.

magnitudes of the gap Δ between the surfaces. In the first series of calculations, a gap was absent, and the absolute slippage condition was specified on the interface; i.e., along the interface, the discontinuity of the shearing stress was equal to zero. These calculations yielded a small (smaller than the experimental perturbation wavelengths) relative displacement of the surfaces due to the lack of shear resistance along the gap. The relative velocity of the surfaces had a pulsed nature ($U = 0.1\text{--}0.2$ mm/ μsec and $\Delta t \approx 0.03 \mu\text{sec}$). For such parameters, the growth of perturbations with the wavelength recorded in the experiments $\lambda \approx 0.7$ mm was inappreciable. Indeed, even in the hydrodynamic approximation [10],

$$a/a_0 \approx \cosh(\Delta U \Delta t 2\pi/\lambda) \approx 1 + (\Delta S \pi/\lambda)^2,$$

where ΔS is the relative displacement of the layer surfaces. In this case, $a/a_0 \approx 1$.

An incorporation of the gap into the computational scheme led to an increase in the rate of the relative displacement of the surfaces even in the case of their absolute friction, i.e., the shearing stress could reach a value $\tau_{\text{max}} \approx 0.5Y_d$. In the calculations with a gap, the yield point was considered low ($Y_d = 0.1$ GPa); i.e., the materials behave themselves as fluids with the equation of state of iron.

Figure 5a gives a curve of the projection of the material's velocity onto the direction of the interface at boundary points of the section versus the coordinate x at the moment when the shock wave traveled a distance $x = 2.25$ cm.

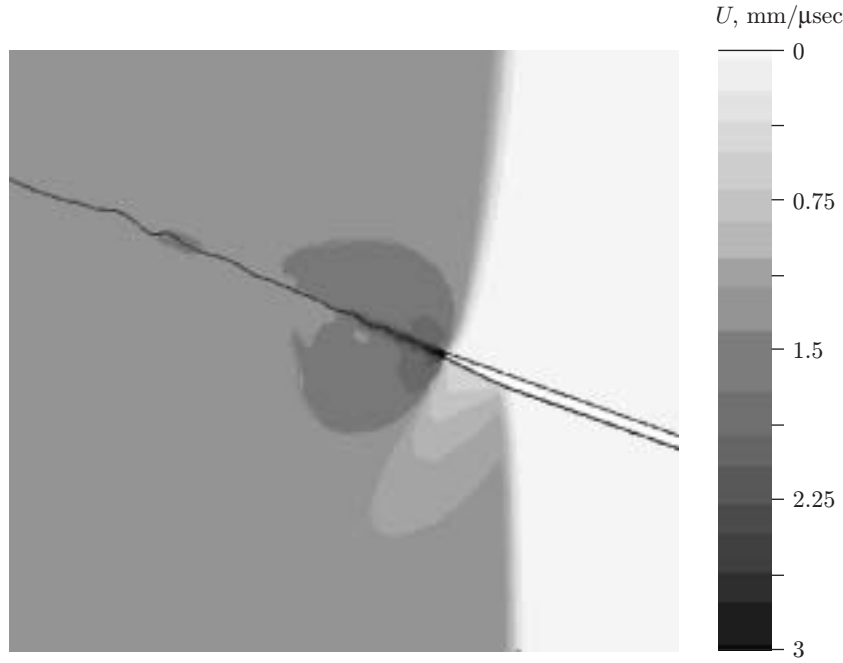


Fig. 6. Fragment of the computational domain at the moment the shock wave traveled a distance $x \approx 2.5$ cm.

The magnitude of the gap $\Delta = 40 \mu\text{m}$ is the maximum possible for articles worked to the sixth class of surface finish and is equal to the total depth of the largest two cavities on the top and bottom plates aligned coaxially.

The maximum velocity is attained directly ahead of the shock-wave front and is $U_{\text{max}} \approx 4 \text{ mm}/\mu\text{sec}$, which is almost four times higher than the mass velocity of the material behind the shock-wave front. The reason for such a velocity jump in the gap is the unloading of the material into the gap. The subsequent closure of the gap and deceleration of the unloaded material leads to a decrease in the velocity to the mean mass velocity $U \approx 1 \text{ mm}/\mu\text{sec}$ in a time $\Delta t \approx 0.15 \mu\text{sec}$. The velocity jump gives rise to a short-term velocity gradient in the direction perpendicular to the interface. Figure 5b shows the material's velocity projection along the interface versus the y coordinate at $x \approx 2.2$ cm, i.e., in the section in which the highest velocity value is observed. From Fig. 5b it follows that in the contact area there is a considerable velocity gradient $\Delta U \approx 3 \text{ mm}/\mu\text{sec}$ in the direction perpendicular to the interface.

In the region separated from the boundary by $\Delta y \approx \pm 0.25$ mm, the velocity gradient reaches a value $\partial U/\partial y \approx 10 \mu\text{sec}^{-1}$. In the remaining region, a velocity gradient is absent. The velocity gradient in the region $\Delta y \approx \pm 0.25$ mm should lead to growth of perturbations whose wavelength is greater than the width of this region, i.e., $\lambda > 0.25$ mm. The calculations predicted the growth of propagation of exactly this wavelength: $\lambda = 0.2\text{--}0.3$ mm. Let us estimate the possible increase in the amplitude of these perturbations over the characteristic time of operation of the velocity gradient pulse $\Delta t \approx 0.15 \mu\text{sec}$ ($\lambda \approx 0.3$ mm and $\Delta U = 3 \text{ mm}/\mu\text{sec}$):

$$a/a_0 \approx \cosh(\Delta U \Delta t \pi/\lambda) \approx 60.$$

Thus, in the hydrodynamic approximation, a considerable growth of perturbations with wavelengths $\lambda > 0.3$ mm is possible. Perturbations with a wavelength $\lambda = 0.7$ mm build up more weakly: $a/a_0 \approx 4$.

Figure 6 presents a fragment of the computational domain at the moment when the shock wave traveled a distance $x \approx 2.5$ cm. From Fig. 6 it follows that closure of the gap gives rise to waves with a characteristic length $\lambda = 0.2\text{--}0.3$ mm, which corresponds to the width of the velocity gradient region and is close to the characteristic dimension of the perturbation at the shock-wave front that results from the presence of the gap.

Calculations with the yield point dependent on pressure and thermal energy were also performed. Such dependences for steel were obtained from results of measurements using the principal stress method [11].

In calculations without assigning initial perturbations, perturbation growth was not observed. Neither did development of perturbation occur when initial sinusoidal perturbations with an amplitude $a_0 = 10 \mu\text{m}$, corresponding to moderate surface finish, and wavelengths $\lambda = 0.46, 0.7,$ and 1.2 mm were assigned on the surface of

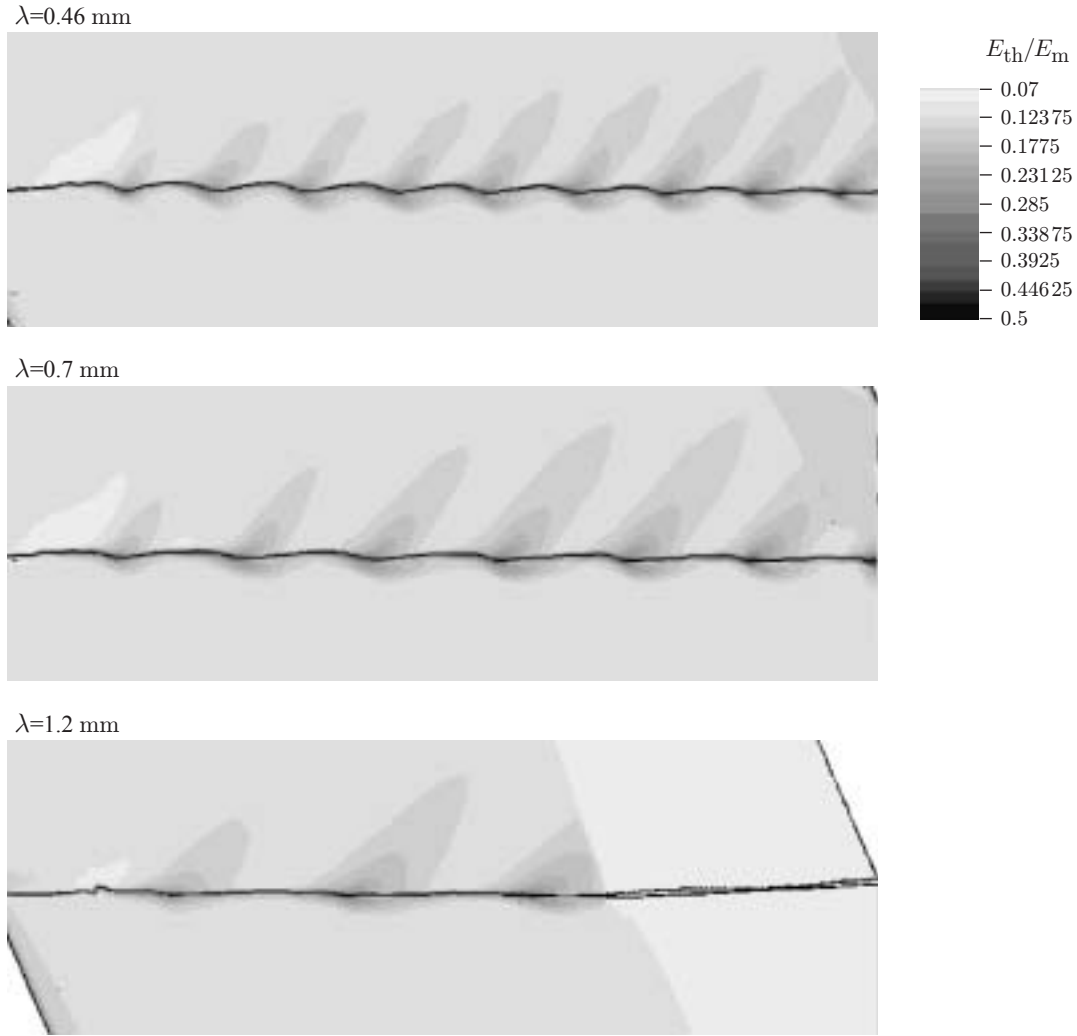


Fig. 7. Fragment of the computational domain with indication of the distribution of the relative thermal energy ($\Delta = 20 \mu\text{m}$).

one of the specimens. Probably, the reason for perturbation growth in a real system is a short-term decrease in shear strength behind the shock-wave front due to the formation of a system of localized shear bands with increased heating.

To verify this hypothesis, we performed calculations in which the yield point was artificially understated and given by

$$Y = 0.045(1 - E_{\text{th}}/E_{\text{m}}) \text{ [GPa]}.$$

In the calculations, perturbations with wavelengths $\lambda = 0.46$ and 0.7 mm increased by a factor of about 2.5. No growth in perturbations with larger wavelength ($\lambda = 1.2$ mm) was observed. In these calculations, the magnitude of the initial gap was $\Delta \approx 20 \mu\text{m}$, which corresponds to the case where one surface having initial perturbations was actually pressed to the other.

Figures 7 and 8 give calculated configurations of the system after shock-wave passage with indication of the distributions of the relative thermal energy $E_{\text{th}}/E_{\text{m}}$ and the plastic strain rate ε , respectively. In the calculations, the width of the large strain zone is close to the experimental value (20–30 μm).

Besides growth in assigned perturbations, the calculations with a gap $\Delta \approx 40 \mu\text{m}$ predicted the occurrence of short-wave perturbations ($\lambda = 0.2\text{--}0.3$ mm), which agrees with the previous calculations without assignment of initial perturbations (Fig. 9).

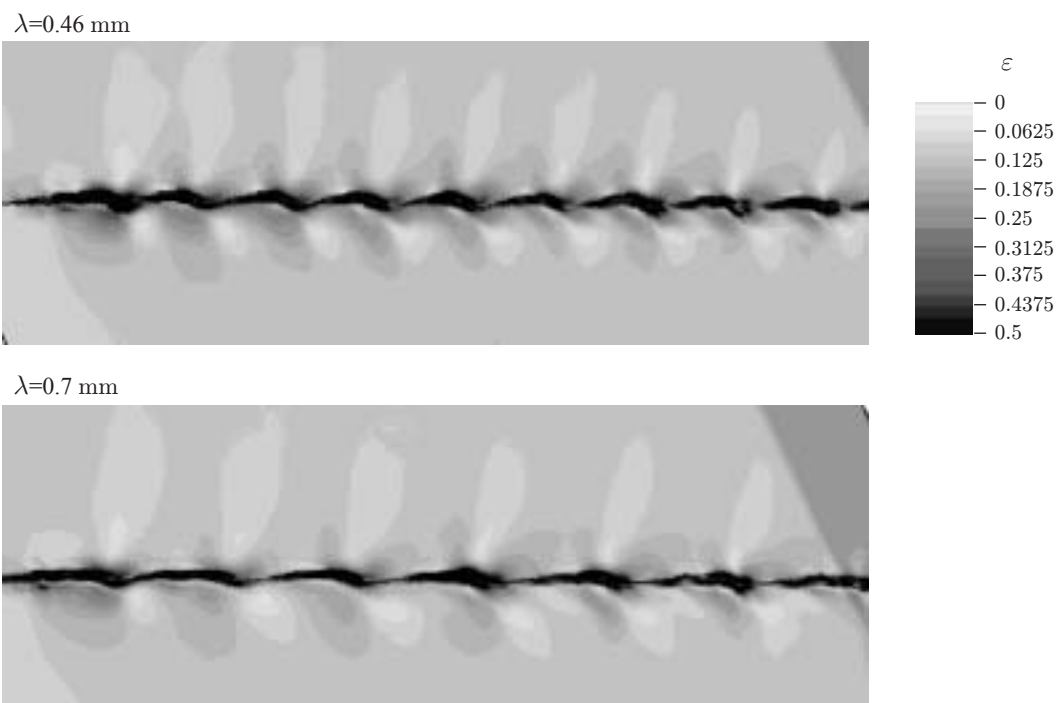


Fig. 8. Fragment of the computational domain with indication of the strain rate distribution ($\Delta = 20 \mu\text{m}$).

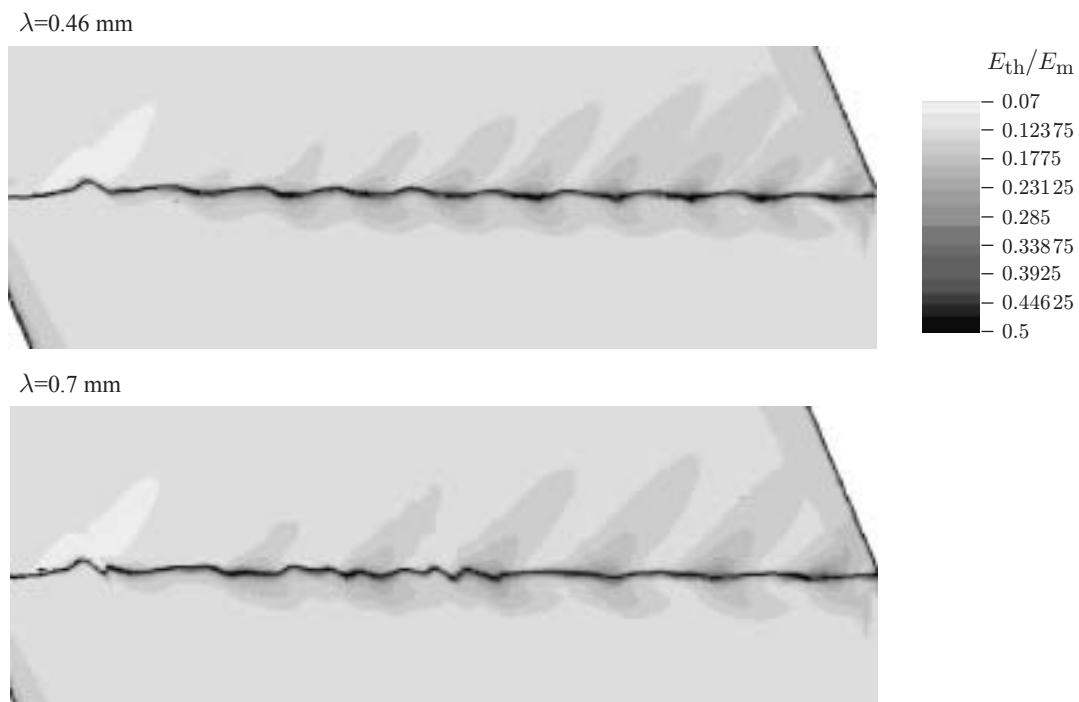


Fig. 9. Fragment of the computational domain with indication of the distribution of the relative thermal energy ($\Delta = 40 \mu\text{m}$).

It should be noted that the probability of instability development exists in the case where the interface between two metals separated by a similar microgap is loaded by a plane shock wave. However, experiments on loading steel plates by a shock wave with the front parallel to the interface at pressure amplitudes $P = 36\text{--}55$ GPa did not reveal development of perturbations on interfaces worked initially to the sixth and lower (to the third class) classes of surface finish; i.e., the magnitude of the gap was $\Delta = 20\text{--}80$ μm .

Obviously, a decrease in the strength of the metal layers in contact during development of large plastic shear strains behind the front of an oblique shock has a significant effect on instability, unlike in the case of loading by a plane shock wave.

Conclusions. Thus, the calculations showed that the most probable reason for the development of perturbations during passage of an oblique shock wave through the interface of identical metals is the presence of a small microgap $\Delta = 20\text{--}40$ μm . The presence of such gaps is possible when the articles are worked to the standard sixth class of surface finish (10 $\mu\text{m} \leq 2a_0 \leq 20$ μm). The gap leads to the occurrence of a considerable but short-term velocity gradient along the interface, which, in turn, is responsible for perturbation propagation. However, to recognize this explanation valid, one should also assume that short-term softening of the material due to the heterogeneous nature of the deformation occurs behind the shock-wave front. It remains to explain the fact that in the experiments, perturbations of a particular wavelength ($\lambda = 0.7$ mm) grow, whereas in the calculations, growth of shorter-wave perturbations ($\lambda = 0.2\text{--}0.3$ mm) is also observed. The calculation yielded a spectrum of perturbation wavelengths, whereas the experiments revealed a single perturbation wavelength.

This work was supported by the Russian Foundation for Fundamental Research (Grant No. 02-01-00796).

REFERENCES

1. H. Birkhoff, *Hydrodynamics. Study in Logic, Fact and Similitude*, Princeton Univ. Press, Princeton (1960).
2. J. Hunt, "Wave formation in explosive welding," *Philos. Mag., Ser. 8*, **17**, No. 148, 669–680 (1968).
3. J. Robinson, "The mechanics of wave formation in impact welding," *Philos. Mag. Ser. 8*, **31**, No. 3, 587–597 (1975).
4. Yu. A. Gordopolov, A. M. Dremine, and A. N. Mikhailov, "Theory of waves on the interface of metals welded by explosion," *Comb. Expl. Shock Waves*, **14**, No. 4, 472–479 (1978).
5. O. B. Drennov, A. L. Mikhailov, P. N. Nizovtsev, and V. A. Raevskii, "Development of perturbations on an interface between metals upon oblique collision with a hypersonic velocity of displacement of the contact point," *Vopr. Atom. Nauki Tekh., Ser. Teor. Prikl. Fiz.*, No. 1, 34–42 (2001).
6. O. B. Drennov, "Development of shear instability in metals," *Zh. Tekh. Fiz.*, **69**, No. 2, 38–42 (1999).
7. O. B. Drennov, "Development of shear instability in media possessing strength," *Khim. Fiz.*, **20**, No. 8, 86–89 (2001).
8. A. S. Dubovik, *Photorecording of Fast Processes* [in Russian], Nauka, Moscow (1984), pp. 77–91.
9. A. I. Abakumov, A. I. Lebedev, and I. A. Nizovtseva, "Rayleigh–Taylor instability in an elastoplastic medium. Numerical investigation," *Vopr. Atom. Nauki Tekh., Ser. Teor. Prikl. Fiz.*, No. 3, 14–19 (1990).
10. L. D. Landau and E. M. Lifshits, *Mechanics of Continua* [in Russian], Gostekhizdat, Moscow (1954), pp. 464–467.
11. Yu. V. Bat'kov, B. L. Glushak, and S. A. Novikov, "Strength of aluminum, copper, and steel at the front of a shock wave," *Comb. Expl. Shock Waves*, **25**, No. 5, 635–640 (1989).